

UNIVERSIDADE ESTADUAL DE CAMPINAS
SISTEMA DE BIBLIOTECAS DA UNICAMP
REPOSITÓRIO DA PRODUÇÃO CIENTÍFICA E INTELECTUAL DA UNICAMP

Versão do arquivo anexado / Version of attached file:

Versão do Editor / Published Version

Mais informações no site da editora / Further information on publisher's website:

<https://link.springer.com/article/10.1007/s11128-016-1409-6>

DOI: 10.1007/s11128-016-1409-6

Direitos autorais / Publisher's copyright statement:

©2016 by Springer. All rights reserved.

DIRETORIA DE TRATAMENTO DA INFORMAÇÃO

Cidade Universitária Zeferino Vaz Barão Geraldo

CEP 13083-970 – Campinas SP

Fone: (19) 3521-6493

<http://www.repositorio.unicamp.br>

Multifractality in fidelity sequences of optimized Toffoli gates

Jalil Khatibi Moqadam¹ · Guilherme S. Welter² ·
Paulo A. A. Esquef²

Received: 5 November 2015 / Accepted: 22 July 2016 / Published online: 29 July 2016
© Springer Science+Business Media New York 2016

Abstract We analyze the multifractality in the fidelity sequences of several engineered Toffoli gates. Using quantum control methods, we consider several optimization problems whose global solutions realize the gate in a chain of three qubits with XY Heisenberg interaction. Applying a minimum number of control pulses assuring a fidelity above 99 % in the ideal case, we design stable gates that are less sensitive to variations in the interqubits couplings. The most stable gate has the fidelity above 91 % with variations about 0.1 %, for up to 10 % variation in the nominal couplings. We perturb the system by introducing a single source of $1/f$ noise that affects all the couplings. In order to quantify the performance of the proposed optimized gates, we calculate the fidelity of a large set of optimized gates under prescribed levels of coupling perturbation. Then, we run multifractal analysis on the sequence of attained fidelities. This way, gate performance can be assessed beyond mere average results, since the chosen multifractality measure (the width of the multifractal spectrum) encapsulates into a single performance indicator the spread of fidelity values around the mean and the presence of outliers. The higher the value of the performance indicator the more concentrated around the mean the fidelity values are and rarer is the occurrence of outliers. The results of the multifractal analysis on the fidelity sequences demonstrate

✉ Jalil Khatibi Moqadam
jalilkhm@hotmail.com

Guilherme S. Welter
gswelter@gmail.com

Paulo A. A. Esquef
pesquef@lncc.br

¹ Instituto de Física “Gleb Wataghin”, Universidade Estadual de Campinas, Campinas, SP, Brazil

² Laboratório Nacional de Computação Científica (LNCC), Petrópolis, RJ, Brazil

the effectiveness of the proposed optimized gate implementations, in the sense they are rendered less sensitive to variations in the interqubits coupling strengths.

Keywords Quantum computation · Quantum control · Time series analysis

1 Introduction

The multifractal formalism describing the scaling of the moments for some distributions in complex systems has been widely used in studying a variety of classical systems [1–10]. Recently, multifractality has also been observed in quantum systems. Quantum wave functions in the Anderson model show multifractality at metal–insulator transition [11–17]. Wave functions in the quantum Hall transition are also multifractal [18–20]. Actually, the strong fluctuations of the wave function amplitude are characterized as wave function multifractality. The relevant normalized measure is the squared modulus of the wave function $|\psi(\mathbf{r})|^2$, and the corresponding moments are $p_q = \int d\mathbf{r} |\psi(\mathbf{r})|^{2q}$, the so-called inverse participation ratios.

Other examples of the multifractal wave functions are certain eigenstates of the quantum baker’s map [21], the eigenfunctions of one dimensional intermediate quantum maps [22], the eigenfunction of Anderson map [23], the Floquet spectrum [24], the electronic states in the Fibonacci superlattice under weak electric fields [25] and the individual wave packets in a periodically kicked system [26]. Moreover, an ensemble of random matrices can be constructed such that the corresponding eigenvectors become multifractal [27–30].

Other measures have also been applied to characterize the multifractality in quantum systems. The Rényi entropy was used to study the multifractality in the ground state wave function in the spin chains [31,32]. The von Neumann entanglement entropy was also used to analyze the multifractality in the wave functions at localization transition [33] as well as in the entanglement of random states [34].

Fractal analysis of periodically kicked quantum systems has been done by means of characterizing the quantum fidelity [35,36], which is defined as the overlap between the perturbed and the unperturbed quantum states $|\langle\psi_\epsilon(t)|\psi(t)\rangle|$. In this case, the fractal properties of a time sequence are analyzed. The object studied here is mathematically different from those mentioned in the above examples, which deal with wave function multifractality.

In this paper, we introduce the gate fidelity $|\text{Tr}[U_\epsilon^\dagger(t)U(t)]|$ to study the multifractality in quantum gates. We, therefore, deal with a sequence of gate implementations whose fidelities, seen as a time sequence, are analyzed in terms of multifractal properties. Specifically the Toffoli gate, a three-qubit gate with central role in quantum information processing is considered here. The gate is realized by applying a sequence of optimized control pulses in a system of three interacting qubits [37]. We perturb the system by adding $1/f$ noise to the interqubit couplings. The pertinence of employing such a degradation noise model has been already discussed in Ref. [38]. We then implement the gate for a large number of noise realizations. The resulted fidelity signal is then analyzed numerically in the multifractal framework, using the formalism recently proposed in Ref. [39].

By manipulating the objective functional in the quantum optimization problem, we design three new gates which show higher degree of multifractality in the fidelity sequence compared with the gate originally proposed in Ref. [37] and with the robust gate designed in Ref. [38]. More specifically, it is shown that, by decreasing the sensitivity of the gate fidelity with respect to variations in the interqubits coupling strengths, the complexity in the implementation of the gate increases and, as a consequence of it, the degree of multifractality in the gate fidelity also increases.

The paper is organized as follows. In Sect. 2, five different realizations of the Toffoli gate are characterized. The multifractal formalism is introduced in Sect. 3. In Sect. 4, the numerical analysis of the multifractality in the fidelity of the Toffoli gate is reported. Finally, the summary and discussions are presented in Sect. 5.

2 The Toffoli gate

The Toffoli gate is an element of the special unitary group $SU(8)$ equal to the identity matrix $\mathcal{I}_{8 \times 8}$ except for the last two rows which are interchanged. It affects three-qubit states belonging to the eight-dimensional Hilbert space \mathbb{C}^8 . The Toffoli gate can be implemented in a system of coupled qubits using different methods. The standard method of implementing the Toffoli gate by decomposing it in terms of the universal gates [40] is not efficient because it leads to a large gate time and low fidelity in the experimental setups [41, 42]. However, an efficient way to implement such multiqubit gate is to implement it directly, by designing a sequence of electromagnetic pulses that affect the qubits and realize the gate [37, 43]. In the following, we consider such an efficient implementation using quantum control methods. We consider a system of three mutually coupled qubits and apply a sequence of optimized pulses that affect all the individual qubits. Suppose the chain of interacting qubits is described by a Heisenberg XY Hamiltonian

$$H_0 = \sum_{m < l} J_{ml} (\sigma_{mx} \sigma_{lx} + \sigma_{my} \sigma_{ly}), \quad m, l = 1, 2, 3 \quad (1)$$

where J_{ml} are the interqubit coupling strengths and σ_{mx} and σ_{my} are Pauli X and Y matrices for qubit m .

The chain of qubits can be manipulated by the control Hamiltonian

$$H_c(t) = \sum_{m=1}^3 \left[u_x^{(m)}(t) \sigma_{mx} + u_y^{(m)}(t) \sigma_{my} \right], \quad (2)$$

where $u_x^{(m)}(t)$ and $u_y^{(m)}(t)$ are two different types of control fields (pulses) affecting the individual qubits.

The system dynamics is therefore governed by the sum of the Hamiltonians in Eqs. (1) and (2). The Schrödinger equation for the unitary operators ($\hbar = 1$)

$$\begin{cases} dU/dt = -i(H_0 + H_c)U \\ U(0) = \mathcal{I}_{8 \times 8}, \end{cases} \quad (3)$$

is used to obtain the evolution operator for the system.

Specifying the control pulses such that the evolution operator in a given time interval t_g implements the Toffoli gate is a numerical optimization problem. Here, the control pulses are considered piecewise-constant functions of time and the gate time t_g is divided into N_t equal pieces accordingly. The Schrödinger equation can then be solved straightforwardly in each time interval. The total time evolution operator is obtained by multiplying the partial time evolution operators in the reverse order. The fidelity is defined as

$$F = \frac{1}{8} \left| \text{Tr} \left[U^\dagger(t_g, N_t, \mathbf{u}, \{J_{ml}\}) U_{\text{Toff}} \right] \right|, \quad (4)$$

where U is the total time evolution of the system during t_g , \mathbf{u} is the concatenation of all control pulses, and U_{Toff} is the Toffoli gate. The values of the control pulses are obtained by solving the optimization problem

$$\max_{\mathbf{u}} F(\mathbf{u}). \quad (5)$$

We obtain five sets of control pulses using fidelity (4) in different optimization problems. The control pulses in each set are optimized such that the resulting gate fidelity functional has a specific response to variations in the interqubit couplings J_{ml} . Each set of control pulses corresponds to a different realization of the Toffoli gate.

The first set of control pulses, \mathbf{u}_1 , is the global solution of problem (5) with $N_t = 20$, $J_{12} = J_{23} = 6J_{13} = \bar{J}$ and $t_g = 4.18\bar{J}^{-1}$. Finding such a set of control pulses has been fully addressed in Ref. [37]. The set is composed of 60 control pulses implementing the Toffoli gate with a fidelity above 99%.

The curve marked with \bullet in Fig. 1 depicts the fidelity (Eq. 4) in terms of J/\bar{J} for the control pulses in the set \mathbf{u}_1 whose elements are optimized for $J = \bar{J}$. The fidelity is clearly high in the vicinity of $J = \bar{J}$ and decreases quickly as J/\bar{J} gets higher or lower than the unity.

The second set of control pulses, \mathbf{u}_2 , is the global solution of the problem

$$\max_{\mathbf{u}} \int_{\bar{J}-\delta J}^{\bar{J}+\delta J} F(\mathbf{u}, J) w(J) dJ, \quad (6)$$

where

$$w(J) = \begin{cases} 0, & \left| \frac{J}{\bar{J}} - 1 \right| \leq \delta_1 \\ 1, & \delta_1 < \left| \frac{J}{\bar{J}} - 1 \right| \leq \delta_2, \end{cases} \quad (7)$$

with $\delta_1 = 0.05$, $\delta_2 = 0.15$ and $\delta J = 0.15\bar{J}$. Here, as before, the same parameters $N_t = 20$, $J_{12} = J_{23} = 6J_{13} = \bar{J}$ and $t_g = 4.18\bar{J}^{-1}$ are used. The set is composed of 60 control pulses implementing the Toffoli gate with a fidelity above 99%, at $J/\bar{J} = 1$. A detailed discussion for optimization problem (6) has been given in Ref. [38].

The curve marked with ▼ in Fig. 1 depicts the fidelity in terms of J/\bar{J} for the set \mathbf{u}_2 . In this case, compared with the fidelity diagram for the set \mathbf{u}_1 , the fidelities are smaller in the vicinity of $J = \bar{J}$, but larger in other points. Applying the pulses in the set \mathbf{u}_2 leads to a Toffoli gate which is less sensitive to the variation in J , specially when $|J/\bar{J} - 1| \leq 0.1$.

In addition to the two sets of control pulses described above, in this work, we design three new sets of control pulses by finding the global solutions of the new optimization problem

$$\max_{\mathbf{u}} \left\{ \beta [F(\mathbf{u}, \bar{J} - J_0) + F(\mathbf{u}, \bar{J}) + F(\mathbf{u}, \bar{J} + J_0)] - |2F(\mathbf{u}, \bar{J}) - F(\mathbf{u}, \bar{J} - J_0) - F(\mathbf{u}, \bar{J} + J_0)| - |F(\mathbf{u}, \bar{J} - J_0) - F(\mathbf{u}, \bar{J} + J_0)| \right\}, \quad (8)$$

where $J_0 = 0.1\bar{J}$. Again, the relation $J_{12} = J_{23} = 6J_{13} = \bar{J}$ is also used. As before, the number of time divisions is set to $N_t = 20$ and the total gate time is fixed to $t_g = 4.18\bar{J}^{-1}$. Setting $\beta \approx 10^3, 10, 0.1$ leads to the sets $\mathbf{u}_3, \mathbf{u}_4$, and \mathbf{u}_5 , respectively. Each set is composed of 60 control pulses that implement the Toffoli gate with a fidelity above 96 %, 93 % and 91 % for the sets $\mathbf{u}_3, \mathbf{u}_4$ and \mathbf{u}_5 , at $J/\bar{J} = 1$, respectively. We can approach the global solution in each optimization by solving the problem with 200 random initial guesses and choosing the fields with highest fidelity.

The main interest in optimization problem (8) is to find those solutions whose fidelity functionals are almost flat in the interval $[\bar{J} - J_0, \bar{J} + J_0]$. Such optimized pulses will realize the Toffoli gate with least sensitivity to perturbations in J . In optimization problem (8), while the first term in the bracket forces the fidelity to have high values in the above interval, the other two terms flatten the fidelity curve in that interval symmetrically. By decreasing the value of β , the fidelity curve becomes more flat in the interval. Specially, for the set \mathbf{u}_5 ($\beta \approx 0.1$), when $|J/\bar{J} - 1| \leq 0.1$, the fidelity varies in [0.918, 0.919], namely a maximum variation of about 0.1 %.

The fidelity curves corresponding to the sets $\mathbf{u}_3, \mathbf{u}_4$ and \mathbf{u}_5 are depicted in Fig. 1 by curves marked with ▲, ◆ and ★, respectively.

Note that there is a compromise between the high fidelity of the gate and the insensitivity of the gate fidelity to the variation in the couplings (stability). In our setup, there is no such a set of control pulses like \mathbf{u}_5 that realize the gate with a stable fidelity around 99 %. In the above method of implementation of the Toffoli gate, we have used a minimum number of control pulses that guarantee a fidelity above 99 % for the perfect situation [37]. In Ref. [43], using the same gate construction, just by increasing the number of pulses, a Toffoli gate with a fidelity above 99.99 % is obtained. Perhaps, an stable gate with higher levels of fidelity can be constructed as well, by increasing the number of control pulses. In this paper, we do not consider such gates which have more that 60 control pulses. However, what we are more interested here is the properties of a fidelity signal which is obtained by large number of implementations of the gate in the disordered system. The above set of gates is sufficient for our purpose.

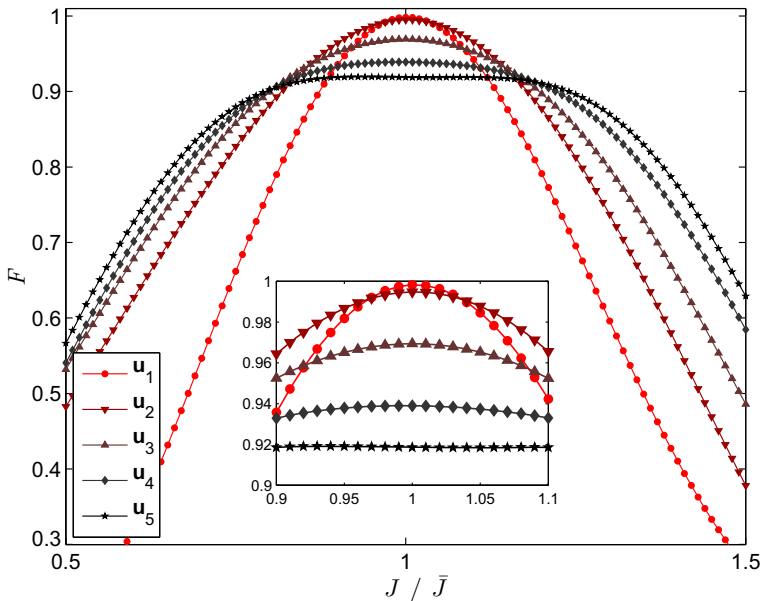


Fig. 1 (Color online) The fidelity (Eq. 4) versus J/\bar{J} for five different sets of control pulses (see the text for the definitions of u_1 to u_5). *Inset* a zoom on the region $|J/\bar{J} - 1| \leq 0.1$

It may be mentioned that piecewise-constant control pulses are convenient from the theoretical point of view. Actually, in reality it is not possible to produce such pulses with an arbitrary accuracy. However, the piecewise-constant control pulses obtained here can be filtered through a low-pass filter to be generated by an actual wave generator. Using a product formula approach [44] (see also [37]), it is possible to obtain the fidelities for the filtered control pulses. In this case, the fidelities are slightly decreased depending on the cutoff frequency of the filter [44].

In Sect. 4, we analyze the multifractality of the fidelity that corresponds to a large number of gate implementations with the above gates.

3 Multifractal analysis

Fractal dimension is an index that informs how detail in a pattern changes depending on the scale it is measured [45], which can be promptly associated to regularity. This way, fractal analysis provides a framework for characterizing and modeling irregular traces and complex shapes found in nature [46, 47]. However, many phenomena that have been identified in physics and applied sciences do exhibit scaling behavior with wild regularity variations which cannot be completely characterized by a single fractal dimension, but with a entire spectrum of fractal dimensions [6, 48]. In face of this difficulty, the multifractal formalism was proposed as a way of characterizing such form of complexity in terms of the scaling properties of singularity measures [2, 49].

The multifractal formalism consists in determining a singularity spectrum $f(\alpha)$, where the singularity strength α accounts for the local regularity and $f(\alpha)$, the Hausdorff dimension of α , gives a geometrical idea of the repartition of these singularities [2, 50].

In general, $f(\alpha)$ is not assessed directly from data but via a scaling function, such as $\zeta(q)$, which is then connected to $f(\alpha)$ by the Legendre transform [49]

$$\alpha = d\zeta(q)/dq, \quad f(\alpha) = \alpha q - \zeta(q) + 1, \quad (9)$$

where $\zeta(q)$ is the power-law exponent of a structure function of order q [49]. It is worth noticing that $\zeta(q)$ is simply related to other widely employed multifractal measures, such as the $\tau(q)$ exponent, the generalized Hurst exponent $h(q)$, and the generalized multifractal dimension $D(q)$ [4, 8, 48, 51].

A number of empirical multifractal formalisms are available in the literature. (For review and comparison of distinct methods c.f. [39, 52–54].) In this study a recently proposed formalism [39], which is briefly described in the sequel, is employed for analysis.

3.1 EMD-DAMF

The EMD-based dominant amplitude multifractal formalism (EMD-DAMF) is a moment-based method. In layman terms, a dominant amplitude multifractal formalism involves initially a multiscale decomposition of the signal of interest. Then, a search for high-magnitude events across different scales is run to form the set of the so-called dominant amplitude coefficients. In the EMD-DAMF, for a given time scale k , the structure functions $S_k(q)$ are defined as the q -order statistical moments of a set of dominant amplitude coefficients $v_{k,\cdot}$, i.e.,

$$S_k(q) := \langle (v_{k,\cdot})^q \rangle = \frac{1}{n_k} \sum_{i=1}^{n_k} (v_{k,i})^q. \quad (10)$$

The dominant amplitude coefficients are obtained via the empirical mode decomposition (EMD) [55], as explained below.

The EMD is a data-driven procedure which decomposes a multicomponent time series $X(t)$ in a relatively small number of multiscale components called intrinsic mode functions (IMFs) and a monotonic trend: $X(t) = \sum_k c_k(t) + r(t)$. Each IMF can be written as $c_k(t) = a_k(t) \cos \varphi_k(t)$, where $a_k(t)$ is a slowly varying amplitude and $\varphi_k(t)$ is the instantaneous phase [55].

One advantage of employing the EMD as a multiscale decomposition is that, thanks to its data-driven formulation, it naturally adapts to signal features and time scales. Moreover, the EMD involves computing signal envelopes so that when an IMF $c_k(t)$ is obtained, $|a_k(t)|$ is already available. Hence, searching for high-magnitude events across different time scales can be accomplished by looking for the local maxima of $|a_k(t)|$. In order to avoid arbitrary small values of amplitude, which could lead to

divergence of negative moments in Eq. (10), the dominant amplitude coefficients are defined as [39]

$$v_{k,i} := \sup_{k' \leq k} \left\{ \max \left(|a_{k'}(t \in I_{k,i})| \right) \right\}, \quad (11)$$

for $k = 1, 2, \dots$, with $i = 1, \dots, n_k$, where n_k is number of local maxima of $a_k(t)$, and $I_{k,i}$ is a time support around the i th maxima of $a_k(t)$.

For processes presenting scaling properties, one can expect that $S_k(q) \simeq \tau_k^{\zeta(q)}$ for $k_{\min} \leq k \leq k_{\max}$, where τ_k is the mean time scale of the k th component. Hence, the singularity spectrum can be estimated from Eq. (9). The choice of the multiresolution coefficients $\{v_k, \cdot\}$ in the EMD-DAMF permits to estimate $\zeta(q)$ even for negative values of q , as with other multifractal formalisms, such as the MFDFA and MFDMA (see [56] and [39] and references therein). As a consequence, it is possible to obtain both sides of the $f(\alpha)$ spectrum [39] (See¹ for a computer program with examples of the EMD-DAMF).

3.2 Singularity spectrum attributes and complexity

Considering the general complexity of engineered quantum gates and their interaction with noise, it is reasonable to expect that fluctuations in the fidelity measured from a sequence of gate implementations may reflect system complexity in some manner.

A typical realization of the fidelity sequence $F(t)$ for the Toffoli gate exhibits an apparent random behavior, as it can be seen in Fig. 2a. Since $F(t)$ is in general a poorly correlated signal, it is advisable to perform multifractal analysis in its integrated path, $X(t) = \int_0^t [F(t') - \langle F \rangle] dt'$, which is shown in Fig. 2b.

The application of the EMD-DAMF method is exemplified in Fig. 3, where one sees in panel (a): the moment function $S_k(q)$ and its scaling behavior; in panel (b): the corresponding scaling exponents $\zeta(q)$, for q between -5 and 5 , in steps of 0.5 ; and, finally, in panel (c): its corresponding singularity spectrum $f(\alpha)$.

The value of α for which $f(\alpha)$ is maximum can be roughly related to the (fractal) Hausdorff dimension of the set [2], and hence, it gives a measure of the apparent smoothness of the process. Small values of α correspond to events with irregular fluctuations, and large values correspond to smoother fluctuations. The spectrum width $\Delta\alpha = \alpha_{\max} - \alpha_{\min}$, on the other hand, quantifies the richness of multifractality, and therefore, $\Delta\alpha$ can be regarded as a measure of complexity. Furthermore, an asymmetric shape of $f(\alpha)$ can be also associated to complexity, since it indicates an unbalanced contribution of singularities [2,57].

4 Multifractal fidelity

Multifractal analysis is the central method in studying complex systems to appreciate of which we have referenced, in the introduction, a large number of works regarding both classical and quantum systems. The approach considered in Sect. 2 for realizing

¹ <http://lps.lncc.br/index.php/demonstracoes/emd-damf>.

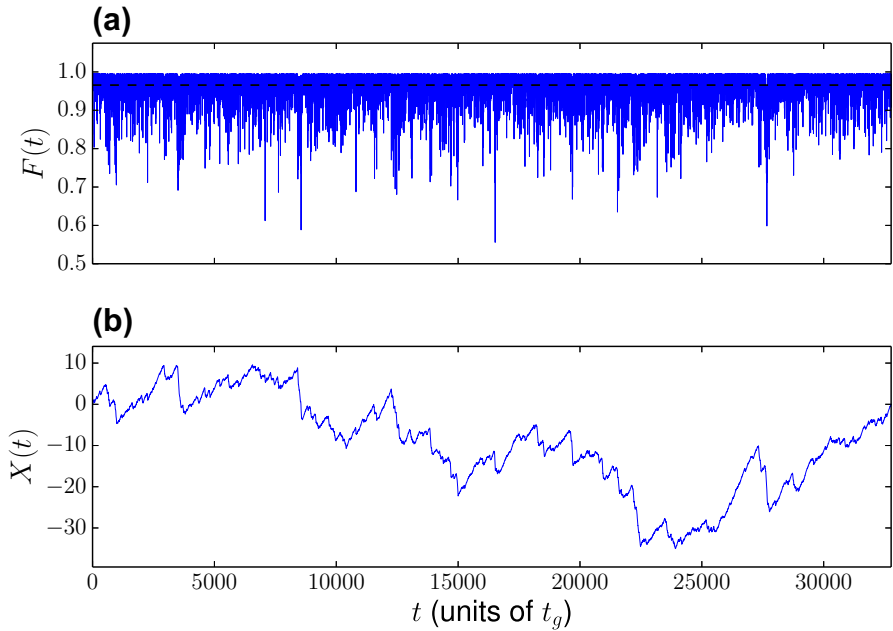


Fig. 2 (Color online) Fidelity time fluctuations $F(t)$ in **a** and its integrated path $X(t) = \int_0^t [F(t') - \langle F \rangle] dt'$ in **b**. The dashed black line in **a** is the mean fidelity $\langle F \rangle$

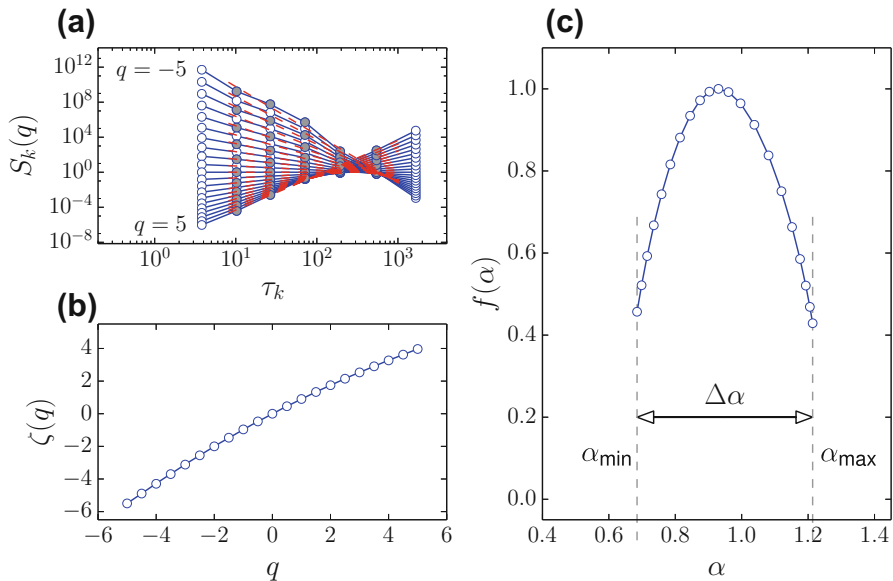


Fig. 3 (Color online) In **a**, the scaling function $S_k(q)$ obtained for the moments $q = -5, -4.5, -4, \dots, 5$ from the integrated fidelity path $X(t)$ shown in Fig. 2b. The dashed red lines in **a** represent the power-law fit of $S_k(q)$ obtained with $k_{\min} = 2$ and $k_{\max} = 6$ for each value of q and, in **b**, their corresponding scaling exponent $\zeta(q)$. Finally, the singularity spectrum $f(\alpha)$, obtained from $\zeta(q)$ through Eq. (9), is shown in **c**

the Toffoli gate implies the evolution of the system is complex. In this section, we investigate such a complex evolution using multifractal analysis.

In Sect. 2, five different sets of control pulses for implementing the Toffoli gate were designed. Here, a sequence of a large number of implementations for each gate is considered and the multifractal properties of the corresponding fidelity sequence is analyzed. Moreover, a static noise is used to perturb the interqubit couplings in each implementation of the gate.

Each gate implementation in the sequence has a fixed lifetime of $t_g = 4.18\bar{J}^{-1}$, as introduced in Sect. 2. In order to treat the problem in the framework of time series analysis, each gate implementation will be indexed by the variable $t_d = t_g d$, with $d \in \mathbb{N}$. For simplicity, henceforth we normalize t_d by t_g and drop the subscript d . Although now t plays the role of a gate implementation index, ordered in time, it shall be clear that each t corresponds to a gate implementation with gate time t_g .

Following the above convention, the couplings are then changed in time as $J_{12} = J_{23} = 6J_{13} = J(t)$. Moreover, noise in the couplings is introduced as

$$J(t) = \bar{J} [1 + \epsilon(t)], \quad (12)$$

where $\epsilon(t)$ is a random sequence of $1/f$ noise with mean $E[\epsilon] = 0$ and variance $E[\epsilon^2] = \sigma^2 < \infty$.

It should be mentioned the implementations of the Toffoli gate discussed in Sect. 2 are specially achievable in a chain of superconducting transmon qubits in circuit QED (see Refs. [37, 38]). It is well known that such superconducting-circuit-based devices are decohered mainly due to degrees of freedom producing $1/f$ noise [58]. In this way, studying the operation of the Toffoli gate when the system is perturbed by the $1/f$ noise is quite pertinent and interesting.

For every realization of $\epsilon(t)$, containing 2^{15} elements, and for a given control pulse \mathbf{u}_k , we obtain 2^{15} values for the fidelity [see Eq. (4)]

$$F^{(k)}(t) = F(J(t), \mathbf{u}_k), \quad (13)$$

one value for each run of the optimized gate with the corresponding $J(t)$.

Figure 4 shows the fidelity sequences for the five sets of control pulses for a fixed realization of the $1/f$ noise with the standard deviation $\sigma = 0.1$. The mean fidelity for each sequence is shown by a dashed black line. The mean fidelity values are about 0.94, 0.96, 0.95, 0.93 and 0.91 % for the sets \mathbf{u}_1 to \mathbf{u}_5 , respectively.

It must be noted that, by just considering the mean fidelities, with $\sigma \leq 0.1$, or by just looking at the fidelity curves in Fig. 1 within the region $|J/\bar{J}| \leq 0.1$, the gates implemented using the pulse sets \mathbf{u}_4 and \mathbf{u}_5 do not show any advantages over the gates implemented with the pulse sets \mathbf{u}_1 to \mathbf{u}_3 . However, the spread of the fidelities around the mean values and the presence of outliers in Fig. 4 are not accounted for in Fig. 1.

In Fig. 4, for proper comparison, the perturbation noise added to the couplings is the same for all shown results. Now, the effect of the different set of control pulses is clearly seen: Despite the reduction of the mean fidelity from \mathbf{u}_2 to \mathbf{u}_5 , the (asymmetrical) variance of the fidelities gets reduced from \mathbf{u}_1 to \mathbf{u}_5 . Therefore, for a given accepted target fidelity, for example not lesser than 91 %, there is a clear advantage in realizing

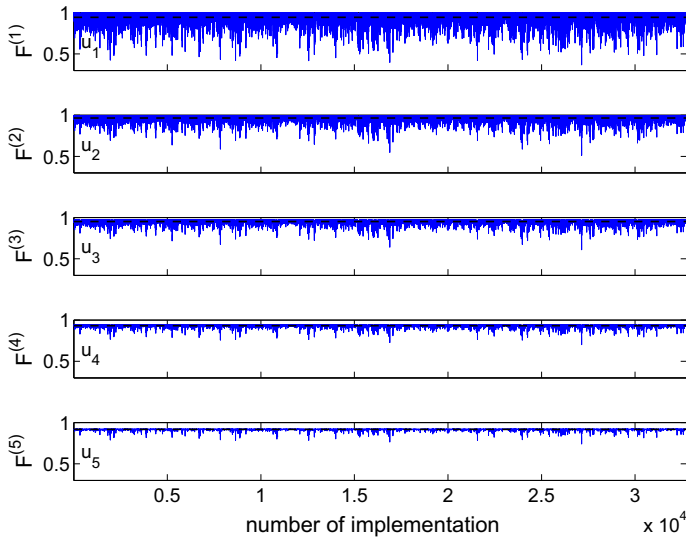


Fig. 4 (Color online) Fidelity sequences for the five different sets of control pulses. Each panel corresponds to 2^{15} gate implementations using the shown set of control pulses. In *all panels*, a fixed realization of the noisy couplings corresponding to the $1/f$ noise with the standard deviation $\sigma = 0.1$ was used (see the text for the definitions of \mathbf{u}_k and $F^{(k)}$). The mean fidelities are shown by *dashed black line* in each *panel*

the gate with the pulse set \mathbf{u}_5 . Therefore, a more complete assessment of the gate performance is needed. For this purpose, in this section, we analyze the multifractal behavior of the sequences of fidelities related to a large number of gate implementations of the above gates.

In brief and superficial terms, multifractal analysis aims at quantifying the occurrence of singular and prominent events that manifest across different scales of observation. In our case, the use of optimized control pulse sets \mathbf{u}_4 and \mathbf{u}_5 has the effect of reducing the spread of fidelity values around the mean value, as can be seen in Fig. 4. Actually, by comparing the fidelity sequences calculated from the pulse sets \mathbf{u}_1 to \mathbf{u}_5 , there seems to be an increase in the contrast among the lowest fidelity values and the mean fidelity. In other words, the lowest fidelity values appear as outliers (prominent singularities) to the otherwise concentrated values around the mean. Therefore, resorting to a multifractal analysis is justified for the performance evaluation problem at hand (Fig. 1), among other equally valid ways to quantify the gate performance.

Before advancing to multifractal analysis of the fidelity sequences, we explain some characteristics of the sequences $F^{(k)}(t)$ by considering the system dynamics in more details. Actually, in our setup the fluctuations in each fidelity sequence are caused by the fluctuations in the interqubit couplings. Moreover, the strength of the fidelity fluctuations is affected by the control fields. Following the explanations given below Eq. (3), the partial evolution of the unperturbed system in the time interval $[(n-1)T, nT]$, where $T = t_g/N_t$ and $n = 1 \dots N_t$, is given by

$$U(T) = \exp[-i(\bar{J}H_{\text{sys}} + H_c)T] \quad (14)$$

where the relation $J_{12} = J_{23} = 6J_{13} = \bar{J}$ is used, and

$$H_{\text{sys}} \equiv (\sigma_{1x}\sigma_{2x} + \sigma_{1y}\sigma_{2y}) + \frac{1}{6}(\sigma_{1x}\sigma_{3x} + \sigma_{1y}\sigma_{3y}) + (\sigma_{2x}\sigma_{3x} + \sigma_{2y}\sigma_{3y}). \quad (15)$$

The total evolution, as mentioned in Sect. 2, is the product of the partial evolutions (14) in reverse order. Now, considering the noise affecting the couplings as given by Eq. (12), the partial evolution of the system in each interval is evaluated as

$$U_\epsilon(T) = \exp\{-i[(1 + \epsilon)\bar{J}H_{\text{sys}} + H_c]T\} \quad (16)$$

where the value of ϵ is supposed to be constant in the whole time interval of length $t_g = TN_t$, within which the partial evolutions are computed. However, ϵ changes its value in each run of the gate and, therefore, the fidelity is changed in each run as well. Equation (16) shows how the control pulses appear in the partial dynamics of the system. It is clear that the fidelity fluctuations depend on both the perturbed couplings and the control fields. In this way, the fluctuations in the fidelity can reflect the complexity of the control pulses, hence, the complexity in the implementation of the gate.

Here, we have to acknowledge several simplifications in our setup with respect to a more realistic set of gate implementations. First of all, by means of the relation $J_{12} = J_{23} = 6J_{13} = \bar{J}$ a single $1/f$ noise realization is used to perturb all the couplings. A more realistic implementation would involve independent sources of perturbations for each coupling.

To model coupling perturbation with independent sources of noise, we can consider a noise with three independent components $\epsilon = (\epsilon_{12}, \epsilon_{13}, \epsilon_{23})$ which affects the couplings as $J_{ij} = \bar{J}_{ij}[1 + \epsilon_{ij}(t)]$, $i, j = 1, 2, 3$, $i < j$. As before, $\epsilon_{ij}(t)$ are (independent) random sequences of $1/f$ noise, with zero mean and equal finite variances, that change their values in each run of the gate but remain constant during the run time t_g . Assuming the couplings satisfy the relation $J_{12} = J_{23} = 6J_{13} = \bar{J}$ on average, the partial evolution of the system in each interval is then given by

$$U_\epsilon(T) = \exp\{-i[\bar{J}(\mathbf{1} + \epsilon) \cdot \mathbf{H}_{\text{sys}} + H_c]T\} \quad (17)$$

where

$$\mathbf{H}_{\text{sys}} \equiv \left(\sigma_{1x}\sigma_{2x} + \sigma_{1y}\sigma_{2y}, \frac{1}{6}(\sigma_{1x}\sigma_{3x} + \sigma_{1y}\sigma_{3y}), \sigma_{2x}\sigma_{3x} + \sigma_{2y}\sigma_{3y} \right), \quad (18)$$

and $\mathbf{1} = (1, 1, 1)$.

Actually, using multiple independent sources of noise with the above properties, namely the same mean, variance and lifetime, just lead to faster decay of the mean fidelity in terms of the standard deviation. This is because the optimization problem corresponding to the pulse sets \mathbf{u}_1 to \mathbf{u}_5 implies the ratio between the three components

in \mathbf{H}_{sys} is kept fixed. The effect of a single source of noise is of the form $\bar{J}(1+\epsilon)\mathbf{1}\cdot\mathbf{H}_{\text{sys}}$ which keeps such ratio fixed. But the effect of three independent sources of noise is of the form $\bar{J}(\mathbf{1}+\epsilon)\cdot\mathbf{H}_{\text{sys}}$ which modifies the ratio between the three components of \mathbf{H}_{sys} in each realization, hence the detrimental effect in the time evolution of the system is stronger (see Sect. IIIB in Ref. [38]). Therefore, for multiple sources of noise, all having the same standard deviation $\sigma = 0.1$, the mean fidelity lines (dashed black lines in Fig. 4) are shifted toward lower levels of fidelity. That is, the variances are larger in this case. Now, if the same level of mean fidelities as the case with a single noise source is desired, the standard deviation should be decreased. Actually, multiple noise sources with a proper standard deviation $\sigma < 0.1$ quantitatively generate the same fidelity sequences as with a single noise source with $\sigma = 0.1$. In this way, Eqs. (16) and (17) basically generate similar sequences. Although, now with lower standard deviations the same multifractal properties as before are expected. A separate simulation may be required to confirm the situation. We do not consider such multiple noise sources in this paper and stress that the simplified perturbation model in Eq. (12) used in our analysis does not reduce the relevance of the reported results. This is because the main objective is to quantify the gate performance in relation to the choice of optimized control pulses.

Other gate implementation parameters, such as the duration of the control pulses and the gate time, are also susceptible to uncertainty. Specially, the noisy gate time can be modeled as $t_g = \bar{t}_g[1 + \epsilon(t)]$ which can also be written as $T = \bar{T}[1 + \epsilon(t)]$ interpreted as an imperfection in the control pulse duration. Here, \bar{t}_g and \bar{T} are the average gate time and the average pulse duration time, respectively. In this case, the partial evolution of the system in each interval is given by

$$\begin{aligned} U_\epsilon(T) &= \exp\{-i(\bar{J}H_{\text{sys}} + H_c)(1 + \epsilon)T\} \\ &= \exp\{-i[(1 + \epsilon)\bar{J}H_{\text{sys}} + (1 + \epsilon)H_c]T\} \end{aligned} \quad (19)$$

which is mathematically equivalent to the situation in which both the couplings and the control pulses are affected by the noise. The noise that affects the optimal control pulses will decrease the average fidelity of the fidelity sequence [44]. However, using the partial dynamics in Eq. (19) may reveal more information about the system and lead to a richer fidelity sequence. We do not consider the evolution (19) in this paper and expect that the simplified scenario (16) we investigate in this section gives sufficient information on the expected average behavior of a set of perturbed Toffoli gates. Actually, in this way, we allow a more clear evaluation of the effect of the designed control pulses on the fidelity in terms of a multifractality measure.

The multifractal nature of the signals $F^{(k)}(t)$ in Eq. (4) is then analyzed by using the EMD-DAMF formalism. We use the width of the multifractal spectrum $\Delta\alpha$ defined as $\alpha(q = 5) - \alpha(q = -5)$, as a measure of the degree of multifractality of the signal. For simplicity, henceforth we will refer to $\Delta\alpha$ as multifractal width. In terms of the problem at hand, the average multifractal width gives a measure of the contrast between the intermittent and regular behavior of the fidelity sequence values. Thus, based on what is seen in Fig. 4, one expects that the fidelity sequence due to the

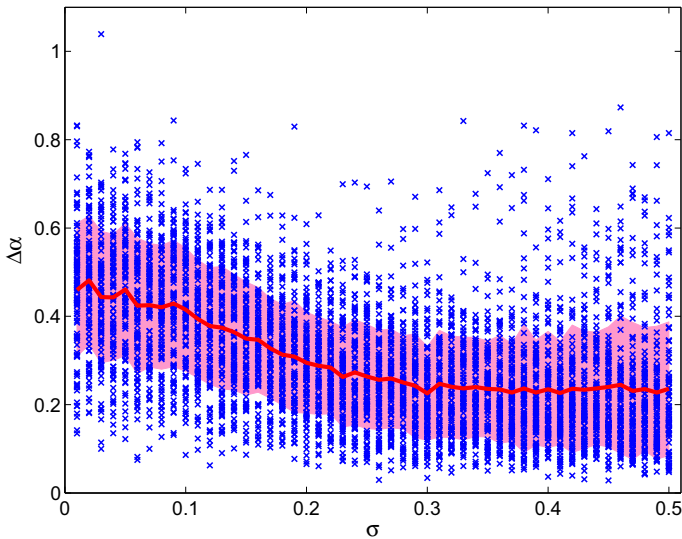


Fig. 5 (Color online) The multifractal width $\Delta\alpha$ versus the standard deviation σ calculated for 100 independent sequences of the fidelity, associated with the control pulses \mathbf{u}_1 , for each standard deviation (\times points). The red solid line shows the average behavior, and the shaded area shows the band of 1 standard deviation around the average

gate \mathbf{u}_5 yields a larger average multifractal width than that related to \mathbf{u}_1 gates. The multifractal analysis is then carried out over different values of σ from 0.01 to 0.5, in steps of 0.01.

We also do statistics by generating $n_r = 100$ independent realizations of $\epsilon(t)$, for each one of the specified values of σ . This way, we can study how the observed average degree of multifractality $\langle\Delta\alpha\rangle$ depends on σ . As explained below, distinct behaviors of the average degree of multifractality can be observed depending on which set of control pulses \mathbf{u}_k is considered in the gate implementation. The behavior of $\langle\Delta\alpha\rangle$ can be interpreted as the complexity of the implementation of the gate. An increasing degree of complexity is observed for those fields implementing the gate with a fidelity with higher tolerance with respect to variations in J .

Figure 5 shows the estimated multifractal width $\Delta\alpha$ versus standard deviation σ , for each of the $n_r = 100$ sequences of the fidelity sequence $F^{(1)}(t)$, which corresponds to the control pulses \mathbf{u}_1 . For any given σ , the set of 100 instances of $\Delta\alpha$'s has its own average $\langle\Delta\alpha\rangle$ and standard deviation. The red solid line depicts $\langle\Delta\alpha\rangle$, and the shaded area shows the band of 1 standard deviation around the average. The number of $\Delta\alpha$ estimates within the band for each σ is larger than 60. The figure shows that the average multifractality decreases when the standard deviation of the noise increases.

Now, we calculate $F^{(k)}(t)$ for the remaining four sets of control pulses, defined in Sect. 2, using the above method systematically. Here, for each set of control pulses, the same ensemble of $n_r = 100$ independent sequences of $J(t)$ is used.

Figure 6 shows $\langle\Delta\alpha\rangle$ as a function of σ for the five sets of control pulses. As can be seen, for $\sigma = 0.1$ the value of $\langle\Delta\alpha\rangle$ increases from \mathbf{u}_1 to \mathbf{u}_5 .

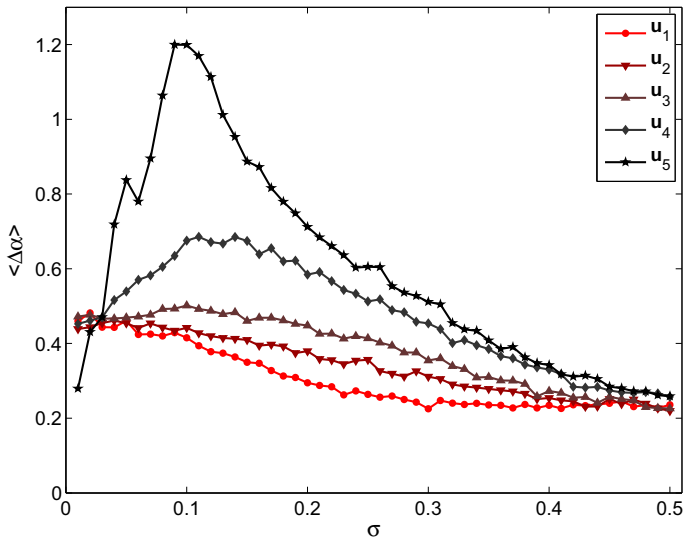


Fig. 6 (Color online) The average multifractal width versus the standard deviation σ for five different sets of control pulses (see the text for the definitions of \mathbf{u}_1 to \mathbf{u}_5)

Here, as regards \mathbf{u}_3 , \mathbf{u}_4 and \mathbf{u}_5 , by reducing β in Eq. (8), respectively, we progressively flattened the fidelity curve in the interval $|J/\bar{J} - 1| \leq 0.1$. As a consequence, we observe an increase in the average multifractal width around $\sigma = 0.1$, from \mathbf{u}_3 to \mathbf{u}_5 . A possible explanation for the observed behavior lies in the more complex control effort associated with \mathbf{u}_5 , when it tries to render $F(J(t), \mathbf{u}_5)$ less sensitive to variations in J around the nominal values. Since F is a function of \mathbf{u} , the complexity of \mathbf{u} carries over to F . The average multifractal widths at $\sigma = 0.1$ for the sets \mathbf{u}_1 to \mathbf{u}_5 are given by 0.4152, 0.4418, 0.5018, 0.6751 and 1.1993, respectively. Therefore, the related value for the set \mathbf{u}_5 increases by a factor of about 2.9 with respect to the set \mathbf{u}_1 . The control pulses in the set \mathbf{u}_5 still implement the Toffoli gate with a fidelity above 91 % which is acceptable [37].

Figure 6 shows that the average multifractality decreases when the noise strength in J increases [59]. Moreover, the curves apparently converge to the same value for sufficiently large σ . A possible explanation for such behaviors of multifractality for large σ would be the following. When the noise variance in J increases well beyond the tolerance J_0 set in Eq. (8), none of the five control pulses, regardless of their complexity, is capable of guaranteeing a well-behaved fidelity in terms of J . Again, since F is a function of both J and \mathbf{u} , it is likely the variance of J which will dominate over the complexity of \mathbf{u} , resulting in a low complexity in F .

Finally, Fig. 6 shows that the multifractality approaches to the same value for small values of standard deviation. In this case, the gate implementation approaches the perfect system gate implementation with noiseless couplings. Therefore, any set of control pulses \mathbf{u}_k implements the gate equally well which reflects in a similar complexity of the fidelity F .

In the above analysis, the correlated $1/f$ noise is used. Now, we briefly report some results on the couplings perturbed by an uncorrelated noise source. If instead of the $1/f$ noise, white Gaussian noise with zero mean is used, similar results to Fig. 6 are attained but generally with slightly lower values of $\Delta\alpha$. However, even in this case, there is still considerable amount of multifractality for the set \mathbf{u}_5 . The curve corresponding to the set \mathbf{u}_5 reaches the maximum $\langle\Delta\alpha\rangle = 0.9936$ at $\sigma = 0.07$, while for the set \mathbf{u}_1 the maximum $\langle\Delta\alpha\rangle = 0.1899$ happened at $\sigma = 0.01$ (not shown). As before, the average multifractality curves decrease when σ increases and apparently converge to the same value for sufficiently large σ which is, however, lower than the converging value for the $1/f$ noise.

It should be mentioned that the 10 % deviation in the couplings which is considered in the above analysis is related to the upper level of the error that is achieved in physical implementations using superconducting quantum information processing devices. The deviations in the values of the relevant parameters (such as Josephson couplings and qubit frequencies in superconducting circuits) are typically on the order of 5–10 % which is indeed inevitable in the state-of-the-art experiments [60,61]. Hence the noise level $\sigma = 10\%$ which appears to be important in our analysis has a direct connection to the real experiments.

The multifractality observed here seems to be of a different origin than in the Anderson transitions that corresponds to localization critical phenomena [12]. Here, the system can tolerate 10 % deviation in the value of the couplings and the gate can be still realized with relatively high fidelity. In the fidelity of the Toffoli gate, as described above, the multifractality reflects the complexity of the control pulses implementing the gate.

5 Summary and discussion

In this paper, we have analyzed the multifractal properties of fidelity sequences related to five different realizations of the Toffoli gate. We considered a system of three coupled qubits described by the Heisenberg XY Hamiltonian. The Toffoli gate can be realized in such a system by applying Zeeman-like control fields (pulses). When defining the fidelity functional, we considered five different optimization problems and found the corresponding global optimized control pulses. All the attained sets of control pulses can implement the Toffoli gate with the fidelity above 91 %, in the noiseless case. However, each set has a different sensitivity to variations in the interqubit couplings.

We realize a large set of imperfect Toffoli gates, whose couplings have been perturbed by $1/f$ noise. The couplings changed in each realization but remained fixed during the gate implementation. Sequences of fidelities related to gates implemented with five different sets of control pulses (\mathbf{u}_1 to \mathbf{u}_5) have been measured for different values of the noise strength. For each of the 100 independent realizations of the fidelity sequence, and for a given standard deviation associated with the couplings, estimates of the average multifractal width $\langle\Delta\alpha\rangle$ of the singularity spectrum $f(\alpha)$ related to the fidelity sequences were obtained via the EMD-DAMF formalism. We found that, for gate sequences implemented with control pulses that flatten the fidelity functional with respect to J around its maximum, one observes an increase in the estimate of

the average multifractal width $\langle \Delta \alpha \rangle$ of the fidelity sequence. The flatter F is around $J = \bar{J}$, the larger the measured average multifractality of F becomes, for J contaminated with $1/f$ noise with standard deviation σ . We observed that for noise with standard deviations above 0.1, the average multifractality tends to decrease with σ and apparently converges to a fixed value for sufficient high σ .

In this paper, a minimum number of control pulses, assuring a fidelity above 99 % in the noiseless situation, are used to implement the Toffoli gate. With such number of control pulses, an stable implementation of the gate (an insensitive gate to variations in the couplings) with almost fixed fidelity around 92 % was designed. However, it is expected an stable gate with higher level of fidelity can be constructed, by increasing the number of control pulses. Such a high-fidelity stable gate and its multifractal properties can be investigated in the same way somewhere else.

To obtain a sequence of fidelities, a large number of gate implementations was considered in which the implementations were affected by a $1/f$ noise. We performed the simulation by considering a single source of noise perturbing the couplings. Using multiple sources of noise disturbing the couplings or noises that influence other part of the system, such as the control pulses, can be explored in the same way.

We observed that by flattening the fidelity curve in the interval $|J/\bar{J} - 1| \leq 0.1$ the average multifractal width peaks around $\sigma = 0.1$. The dependence of the peak position to the length of such interval may be investigated in a different work.

Intuitively, one could say that \mathbf{u}_5 is the most specialized control sequence for the case when $|J/\bar{J} - 1| < 0.1$. A good question would be whether the increase in the multifractality of \mathbf{u}_5 around $\sigma = 0.1$ could be interpreted as a measure of its specialization.

We speculate that the changes in the richness of multifractality observed here are a result of the complexity in the implementation of the gate. The effects of the number of control pulses may be analyzed to see whether there is a critical number for the control pulses below which no multifractality can be observed. The approach that is given in Sect. 2 for implementing the Toffoli gate is a standard way in quantum control theory in engineering quantum gates. Therefore, the multifractality behavior of the fidelity observed here is also expected in other engineered gates. Specially, it is interesting to check the multifractality for the $CNOT$ gate which is less complex.

Acknowledgments JKM acknowledges Grants PCI-DB 302866/2014-0 and PDJ 165941/2014-6, and GSW and PAEE acknowledge Grant 475566/2012-2, from Brazilian National Council for Scientific and Technological Development (CNPq).

References

1. Mandelbrot, B.B.: Intermittent turbulence in self-similar cascades: divergence of high moments and dimension of the carrier. *J. Fluid Mech.* **62**(02), 331–358 (1974)
2. Halsey, T., Jensen, M., Kadanoff, L., Procaccia, I., Shraiman, B.: Fractal measures and their singularities: the characterization of strange sets. *Phys. Rev. A* **33**(2), 1141 (1986)
3. Meneveau, C., Sreenivasan, K.: The multifractal nature of turbulent energy dissipation. *J. Fluid Mech.* **224**, 429–484 (1991)
4. Muzy, J., Bacry, E., Arnéodo, A.: Wavelets and multifractal formalism for singular signals: application to turbulence data. *Phys. Rev. Lett.* **67**(25), 3515–3518 (1991)

5. Mandelbrot, B., Fisher, A., Calvet, L.: A multifractal model of asset returns. Cowles Foundation Discussion Papers (1997)
6. Stanley, H., Meakin, P.: Multifractal phenomena in physics and chemistry. *Nature* **335**(6189), 405–409 (1988)
7. Abry, P., Baraniuk, R., Flandrin, P., Riedi, R., Veitch, D.: Multiscale nature of network traffic. *IEEE Signal Proc. Mag.* **19**(3), 28–46 (2002)
8. Jafari, G., Pedram, P., Hedayatifar, L.: Long-range correlation and multifractality in Bach's inventions pitches. *J. Stat. Mech: Theory Exp.* **2007**(04), P04012 (2007)
9. Lovejoy, S., Schertzer, D.: Haar wavelets, fluctuations and structure functions: convenient choices for geophysics. *Nonlinear Process. Geophys.* **19**, 513–527 (2012)
10. Ausloos, M.: Generalized hurst exponent and multifractal function of original and translated texts mapped into frequency and length time series. *Phys. Rev. E* **86**(3), 031108 (2012)
11. Mirlin, A.D.: Statistics of energy levels and eigenfunctions in disordered systems. *Phys. Rep.* **326**(5), 259–382 (2000)
12. Evers, F., Mirlin, A.D.: Anderson transitions. *Rev. Mod. Phys.* **80**, 1355–1417 (2008)
13. Rodriguez, A., Vasquez, L.J., Römer, R.A.: Multifractal analysis with the probability density function at the three-dimensional Anderson transition. *Phys. Rev. Lett.* **102**, 106406 (2009)
14. Rodriguez, A., Vasquez, L.J., Roemer, R.A.: Optimisation of multifractal analysis at the 3D Anderson transition using box-size scaling. *Eur. Phys. J. B Condens. Matter Complex Syst.* **67**(1), 77–82 (2009)
15. Rodriguez, A., Vasquez, L.J., Slevin, K., Römer, R.A.: Critical parameters from a generalized multifractal analysis at the Anderson transition. *Phys. Rev. Lett.* **105**, 046403 (2010)
16. Rodriguez, A., Vasquez, L.J., Slevin, K., Römer, R.A.: Multifractal finite-size scaling and universality at the Anderson transition. *Phys. Rev. B* **84**, 134209 (2011)
17. Burmistrov, I.S., Gornyi, I.V., Mirlin, A.D.: Multifractality at Anderson transitions with Coulomb interaction. *Phys. Rev. Lett.* **111**, 066601 (2013)
18. Huckestein, B.: Scaling theory of the integer quantum hall effect. *Rev. Mod. Phys.* **67**, 357–396 (1995)
19. Evers, F., Mildenberger, A., Mirlin, A.D.: Multifractality of wave functions at the quantum hall transition revisited. *Phys. Rev. B* **64**, 241303 (2001)
20. Evers, F., Mildenberger, A., Mirlin, A.D.: Multifractality at the spin quantum hall transition. *Phys. Rev. B* **67**, 041303 (2003)
21. Meenakshisundaram, N., Lakshminarayan, A.: Multifractal eigenstates of quantum chaos and the Thue–Morse sequence. *Phys. Rev. E* **71**, 065303 (2005)
22. Martin, J., Giraud, O., Georgeot, B.: Multifractality and intermediate statistics in quantum maps. *Phys. Rev. E* **77**, 035201 (2008)
23. Martin, J., García-Mata, I., Giraud, O., Georgeot, B.: Multifractal wave functions of simple quantum maps. *Phys. Rev. E* **82**, 046206 (2010)
24. Bandyopadhyay, J.N., Wang, J., Gong, J.: Generating a fractal butterfly Floquet spectrum in a class of driven SU(2) systems: eigenstate statistics. *Phys. Rev. E* **81**, 066212 (2010)
25. Wołoszyn, M., Spisak, B.J.: Multifractal analysis of the electronic states in the Fibonacci superlattice under weak electric fields. *Eur. Phys. J. B Condens. Matter Complex Syst.* **85**(1), 1–7 (2012)
26. García-Mata, I., Martin, J., Giraud, O., Georgeot, B.: Multifractality of quantum wave packets. *Phys. Rev. E* **86**, 056215 (2012)
27. Mirlin, A.D., Fyodorov, Y.V., Dittes, F.M., Quezada, J., Seligman, T.H.: Transition from localized to extended eigenstates in the ensemble of power-law random banded matrices. *Phys. Rev. E* **54**, 3221–3230 (1996)
28. Kravtsov, V.E., Muttalib, K.A.: New class of random matrix ensembles with multifractal eigenvectors. *Phys. Rev. Lett.* **79**, 1913–1916 (1997)
29. Bogomolny, E., Giraud, O.: Multifractal dimensions for all moments for certain critical random-matrix ensembles in the strong multifractality regime. *Phys. Rev. E* **85**, 046208 (2012)
30. Fyodorov, Y.V., Ossipov, A., Rodriguez, A.: The anderson localization transition and eigenfunction multifractality in an ensemble of ultrametric random matrices. *J. Stat. Mech: Theory Exp.* **2009**(12), L12001 (2009)
31. Atas, Y.Y., Bogomolny, E.: Multifractality of eigenfunctions in spin chains. *Phys. Rev. E* **86**, 021104 (2012)
32. Luitz, D.J., Alet, F., Laflorencie, N.: Universal behavior beyond multifractality in quantum many-body systems. *Phys. Rev. Lett.* **112**, 057203 (2014)

33. Jia, X., Subramaniam, A.R., Gruzberg, I.A., Chakravarty, S.: Entanglement entropy and multifractality at localization transitions. *Phys. Rev. B* **77**, 014208 (2008)
34. Giraud, O., Martin, J., Georgeot, B.: Entropy of entanglement and multifractal exponents for random states. *Phys. Rev. A* **79**, 032308 (2009)
35. Pellegrini, F., Montangero, S.: Fractal fidelity as a signature of quantum chaos. *Phys. Rev. A* **76**(5), 052327 (2007)
36. Bin, Y., Gang, D., Xiao-Ping, M.: Fractals in the open quantum kicked top model. *Commun. Nonlinear Sci. Numer. Simul.* **15**(10), 2967–2973 (2010)
37. Stojanović, V.M., Fedorov, A., Wallraff, A., Bruder, C.: Quantum-control approach to realizing a Toffoli gate in circuit QED. *Phys. Rev. B* **85**(5), 054504 (2012)
38. Moqadam, J.K., Portugal, R., Svaiter, N.F., de Oliveira Corrêa, G.: Analyzing the Toffoli gate in disordered circuit QED. *Phys. Rev. A* **87**, 042324 (2013)
39. Welter, G.S., Esquef, P.A.A.: Multifractal analysis based on amplitude extrema of intrinsic mode functions. *Phys. Rev. E* **87**, 032916 (2013)
40. Nielsen, M.A., Chuang, I.L.: *Quantum Computation and Quantum Information*. Cambridge University Press, New York (2010)
41. Monz, T., Kim, K., Hänsel, W., Riebe, M., Villar, A.S., Schindler, P., Chwalla, M., Hennrich, M., Blatt, R.: Realization of the quantum Toffoli gate with trapped ions. *Phys. Rev. Lett.* **102**, 040501 (2009)
42. Lanyon, B.P., Barbieri, M., Almeida, M.P., Jennewein, T., Ralph, T.C., Resch, K.J., Pryde, G.J., Obrien, J.L., Gilchrist, A., White, A.G.: Simplifying quantum logic using higher-dimensional Hilbert spaces. *Nat. Phys.* **5**(2), 134–140 (2009)
43. Zahedinejad, E., Ghosh, J., Sanders, B.C.: High-fidelity single-shot Toffoli gate via quantum control. *Phys. Rev. Lett.* **114**, 200502 (2015)
44. Heule, R., Bruder, C., Burgarth, D., Stojanović, V.M.: Local quantum control of Heisenberg spin chains. *Phys. Rev. A* **82**, 052333 (2010)
45. Mandelbrot, B.B.: *The Fractal Geometry of Nature*. W. H. Freeman, New York (1982)
46. Mandelbrot, B., Van Ness, J.: Fractional Brownian motions, fractional noises and applications. *SIAM Rev.* **10**(4), 422–437 (1968)
47. Voss, R.F.: Random fractals: self-affinity in noise, music, mountains, and clouds. *Phys. D* **38**(1), 362–371 (1989)
48. Arnéodo, A., Bacry, E., Muzy, J.: The thermodynamics of fractals revisited with wavelets. *Phys. A* **213**(1), 232–275 (1995)
49. Parisi, G., Frisch, U.: Fully developed turbulence and intermittency. In: Ghil, M., Benzi, R., Parisi, G. (eds.) *Turbulence and Predictability in Geophysical Fluid Dynamics and Climate Dynamics*, pp. 84–88. North Holland, Amsterdam (1985)
50. Barral, J., Seuret, S.: From multifractal measures to multifractal wavelet series. *J. Fourier Anal. Appl.* **11**(5), 589–614 (2005)
51. Kantelhardt, J., Zschiegner, S., Koscielny-Bunde, E., Havlin, S., Bunde, A., Stanley, H.: Multifractal detrended fluctuation analysis of nonstationary time series. *Phys. A* **316**(1), 87–114 (2002)
52. Turiel, A., Pérez-Vicente, C., Grazzini, J.: Numerical methods for the estimation of multifractal singularity spectra on sampled data: a comparative study. *J. Comput. Phys.* **216**(1), 362–390 (2006)
53. Oświęcimka, P., Kwapień, J., Drożdż, S.: Wavelet versus detrended fluctuation analysis of multifractal structures. *Phys. Rev. E* **74**(1), 016103 (2006)
54. Huang, Y., Schmitt, F., Hermand, J., Gagne, Y., Lu, Z., Liu, Y.: Arbitrary-order Hilbert spectral analysis for time series possessing scaling statistics: comparison study with detrended fluctuation analysis and wavelet leaders. *Phys. Rev. E* **84**(1), 016208 (2011)
55. Huang, N., Shen, Z., Long, S., Wu, M., Shih, H., Zheng, Q., Yen, N., Tung, C., Liu, H.: The empirical mode decomposition and the Hilbert spectrum for nonlinear and non-stationary time series analysis. *Philos. Trans. R. Soc. A* **454**(1971), 903–995 (1998)
56. Mantica, G.: The global statistics of return times: return time dimensions versus generalized measure dimensions. *J. Stat. Phys.* **138**(4–5), 701–727 (2010)
57. Shimizu, Y., Thurner, S., Ehrenberger, K.: Multifractal spectra as a measure of complexity in human posture. *Fractals* **10**(01), 103–116 (2002)
58. Paladino, E., Galperin, Y.M., Falci, G., Altshuler, B.L.: $1/f$ noise: implications for solid-state quantum information. *Rev. Mod. Phys.* **86**, 361–418 (2014)
59. Dubertrand, R., García-Mata, I., Georgeot, B., Giraud, O., Lemarié, G., Martin, J.: Two scenarios for quantum multifractality breakdown. *Phys. Rev. Lett.* **112**, 234101 (2014)

60. Tsomokos, D., Hartmann, M., Huelga, S., Plenio, M.: Entanglement dynamics in chains of qubits with noise and disorder. *New J. Phys.* **9**(3), 79 (2007)
61. Tsomokos, D.I., Ashhab, S., Nori, F.: Fully connected network of superconducting qubits in a cavity. *New J. Phys.* **10**(11), 113020 (2008)